# The Reaction of Nitrogen with Dilute Solutions of Barium in Liquid Lithium: Electrical Resistivity, X-Ray Phase Analysis, Kinetic and Thermal Analysis Studies

**Peter Hubberstey and Peter G. Roberts**
*Chemistry Department, University of Nottingham, Nottingham NG7 2RD, UK*

The reaction of nitrogen with liquid lithium containing dissolved barium which follows a solution–precipitation mechanism has been studied. Initially, nitrogen dissolves in the liquid metal to form an homogeneous solution; the reaction is first order with respect to nitrogen with an activation energy of 33.6 kJ $mol^{-1}$. Subsequently, it reacts to form a precipitate of $Li_3N$; the $Li_3N$ crystallisation face is dependent on the barium content of the solution, nitrogen solubility rising with increasing barium content. The ternary nitride, LiBaN, is only formed on cooling the solution; there is no evidence for $Ba_2N$ or $Ba_3N_2$ formation. This behaviour contrasts with that in the corresponding Na–M–N (M = Sr or Ba) systems where the solubility is directly proportional to the alkaline-earth metal content of the solution and the precipitating phase is the alkaline-earth metal subnitride, $M_2N$ (M = Sr or Ba). Analysis of the crystallisation fields of Li, $Li_4Ba$, LiBaN and $Li_3N$ indicated they are separated by monovariant curves which fall from the binary eutectics (Li–Ba, $x_{Ba}$ = 0.105 and 416 K; Li–N, degenerate at 453.5 K, $Li_3N$–LiBaN, unknown) through a quasi-peritectic equilibrium involving liquid, lithium, $Li_4Ba$ and LiBaN (372 K) to a ternary eutectic point based on liquid, lithium, $Li_3N$ and LiBaN (368 K).

The solvent chemistry of the lighter liquid alkali metals (lithium and sodium) is fairly well established.[1] Reactions between metals (M), either dissolved in or immersed in liquid alkali metals (A), and non-metals (X) result in one of three products, depending on their thermodynamic stabilities; the ternary salt $A_pM_qX_r$, the binary alkali-metal salt, $A_pX_r$ or the binary metal salt, $M_qX_r$. In the former two cases, the alkali metal plays an active role in the chemistry; in the latter case it acts as an inert solvent.

Reactions involving oxygen and nitrogen have been studied in particular detail. Lithium oxide is so thermodynamically stable [$\Delta G_f°$ ($Li_2O$, c, 298 K) = −562.1 kJ $mol^{-1}$][2] that it is the sole product of Li–M–O systems even in the presence of reactive metals (*e.g.*, chromium, iron or nickel).[3] Sodium oxide, on the other hand, is considerably less stable [$\Delta G_f°$ ($Na_2O$, c, 298 K) = −379.1 kJ $mol^{-1}$][2] and although $Na_2O$ is the sole product of the Na–Ni–O system,[4] the corresponding Na–Cr–O system also yields the ternary oxide, $NaCrO_2$.[5] The thermodynamic stability of lithium nitride [$\Delta G_f°$ ($Li_3N$, c, 298 K) = −128.6 kJ $mol^{-1}$][2] is such that nitrogen dissolved in liquid lithium behaves similarly to oxygen dissolved in liquid sodium. Thus, the ternary nitrides $Li_5SiN_3$,[6–8] $Li_7VN_4$[9] and $Li_9CrN_5$[8,10] are formed in the Li–M–N (M = Si, V or Cr) systems but lithium nitride is the sole product of the Li–Sn–N and Li–Pb–N systems.[11] Since sodium nitride is unstable,[12,13] the solvent necessarily acts as an inert reaction medium in Na–M–N systems. For example, the binary metal nitrides $M_2N$ (M = Sr or Ba)[14–17] are formed in the Na–M–N (M = Sr or Ba) systems. It is noteworthy that binary metal salts, $M_qX_r$, are only formed when ternary salts, $A_pM_qX_r$, are not thermodynamically favoured [*e.g.*, Na–M–N (M = Sr or Ba) systems]; if both are potential products [*e.g.*, Na–M–O and Li–M–N systems] the ternary salts are formed exclusively, confirming their greater thermodynamic stability.[18]

Since the reaction products in these systems are determined by the thermodynamic activity of the alkali metal, diluting the latter by alloy formation can change the reaction chemistry.[19] Recent experiments on the solution properties of Pb–17Li (a Pb–Li alloy containing 17 atom% Li presently being considered for use as tritium breeder in fusion reactor systems[20,21]) have shown that the lithium activity in this system is so low that oxygen, which solely forms $Li_2O$ in the Li–Cr–O system, corrodes chromium forming $LiCrO_2$,[22] while nitrogen, which forms $Li_9CrN_5$ in the Li–Cr–N system, is totally unreactive.[19]

The formation of the binary metal nitrides $M_2N$ (M = Sr or Ba)[14–17] in the Na–M–N (M = Sr or Ba) systems is one of the rare examples in which the solvent acts as an inert reaction medium, presumably owing to the instability of $Na_3N$. For the Na–Ba–N system, resistivity[16] and solubility[15] studies of the solutions coupled with X-ray powder diffraction studies of the solid products[14] indicated that an initial solution process is followed by precipitation of $Ba_2N$ which, in the presence of excess nitrogen, reacts further to form $Ba_3N_2$. Since the extent of the solution process is determined solely by the amount of barium dissolved in the liquid sodium, precipitation commencing at a Ba : N ratio of ≈4 : 1, it has been suggested[23] that the nitrogen, which is effectively insoluble in liquid sodium,[24] is solvated by the barium forming a soluble $Ba_4N$ species. Independent evidence for such a species has been recently reported by Rauch and Simon[25] who described the isolation and characterisation (by single-crystal X-ray diffraction methods) of $NaBa_3N$. The reaction sequence, which can be summarised by equations (1)–(3) has also been shown[14] to be

$$8[Ba]_{(Na)} + N_2(g) \longrightarrow 2['Ba_4N']_{(Na)} \quad (1)$$

$$2['Ba_4N']_{(Na)} + N_2(g) \longrightarrow 4Ba_2N(s) \quad (2)$$

$$6Ba_2N(s) + N_2(g) \longrightarrow 4Ba_3N_2(s) \quad (3)$$

compatible with a simple Na–Ba–N ternary phase diagram dominated by a very steep $Ba_2N$ precipitation face with an effectively constant Ba : N molar ratio of ≈4 : 1.

Analogous experiments[17] on the Na–Sr–N system showed a similar behaviour pattern, the only difference being a more limited solution process, precipitation of $Sr_2N$ starting at a Sr : N molar ratio of ≈17 : 1.

Since lithium forms a stable nitride, $Li_3N$, the Li–M–N (M = Ca, Sr or Ba) systems might exhibit contrasting chemistry. Feasible reaction products are $M_2N$ (M = Ca, Sr or Ba), the

lithium acting as an inert solvent, or LiMN or $Li_3N$, the lithium adopting an active role. We now report in detail the results of a study of the Li–Ba–N system undertaken using a combination of electrical resistivity, X-ray phase, kinetic and thermal analyses.

*The* Li–Ba–N *Ternary System.*—Although the reaction system under study nominally forms part of the Li–Ba–N ternary system, it is best to consider it within the Li–Ba–$Ba_3N_2$–$Li_3N$ pseudo-quaternary system. Phase relationships therein have been little studied, the only data available relating to its four constituent binary systems. To permit interpretation of the results of the present investigation, it is thus necessary to speculate on the form of the phase diagram. A space model (isothermal contour diagram), based on the phase relationships of the constituent binary systems and consistent with the results described here is presented in Fig. 1. The Li–Ba binary system[26,27] is based on a eutectic (Fig. 1); it contains one intermetallic phase, $Li_4Ba$, which forms from a peritectic reaction at 429 K. The hypoeutectic liquidus falls from the melting point of pure lithium (453.5 K) to the eutectic between lithium and $Li_4Ba$ ($x_{Ba}$ = 0.105, $T$ = 416 K); the hypereutectic liquidus then rises gently to the peritectic reaction ($x_{Ba}$ = 0.184, $T$ = 429 K) before rising more steeply to the melting point of barium (998 K).

One intermediate phase, $Ba_2N$, exists in the Ba–$Ba_3N_2$ system (Fig. 1), which is based on a eutectic ($x_N$ = 0.144, $T$ = 781 K). As phase relationships have only been studied up to $x_N$ = 0.25,[28] the thermal properties of $Ba_2N$ and $Ba_3N_2$ are unknown. However, the thermodynamics of the decomposition of $Ba_3N_2$, equation (4), have been elucidated by two

$$Ba_3N_2(s) \rightleftharpoons \tfrac{3}{2}Ba_2N(s) + \tfrac{1}{4}N_2(g) \qquad (4)$$

independent workers.[29,30] The quoted $\Delta H°$ values (41.7 kJ $mol^{-1}$ at 950 K[29] and 36.8 kJ $mol^{-1}$ at 298 K[30]), although not directly comparable, indicate the greater thermodynamic stability of $Ba_3N_2$ with respect to $Ba_2N$. Thus in the quaternary diagram (Fig. 1) $Ba_2N$ is assumed to form *via* a peritectic reaction involving $Ba_3N_2$ and a barium-rich liquid. This assumption is not significant in the present context, as our principal interest in the ternary system lies in the lithium-rich corner of the diagram.

Little is known of $Ba_3N_2$–$Li_3N$ phase relationships, except for the synthesis and structural characterisation of the ternary compound, LiBaN.[31] Its stability is evidenced by the fact that it has been synthesised by high temperature reaction of nitrogen with equimolar Li–Ba mixtures and with solutions of Li–Ba mixtures dissolved in liquid sodium.[32] The present results suggest that LiBaN should be shown in the quaternary phase system as a congruently melting compound which exists over a wide composition range (Fig. 1).

The Li–$Li_3N$ phase diagram (Fig. 1) is a simple eutectic;[33–35] the eutectic lies close to the lithium axis ($x_N$ = 0.000 68, $T$ = 453.24 K),[36] the hypereutectic liquidus rising steeply from the eutectic temperature to the melting point of $Li_3N$ (1086 K).

Since the present study is concerned solely with dilute solutions of both barium and nitrogen, it is the lithium corner of the pseudo-quaternary phase diagram (Fig. 1) which is of particular interest. This region of the space model is dominated by the divariant precipitation faces of lithium, $Li_4Ba$, barium, LiBaN and $Li_3N$. Those of $Li_4Ba$, barium and LiBaN intersect forming a series of monovariant lines ($p_1P_2$, $S_1P_2$, $P_1P_2$) which meet at a pseudo-peritectic point ($P_2$). Those of lithium, $Li_4Ba$ and LiBaN do likewise forming three monovariant lines ($e_1P_1$, $P_2P_1$, $E_1P_1$) which meet at a second pseudo-peritectic point ($P_1$). The precipitation faces of lithium, LiBaN and $Li_3N$ intersect forming a series of monovariant lines ($e_2E_1$, $e_3E_1$, $P_1E_1$) which meet at an invariant ternary eutectic point ($E_1$).

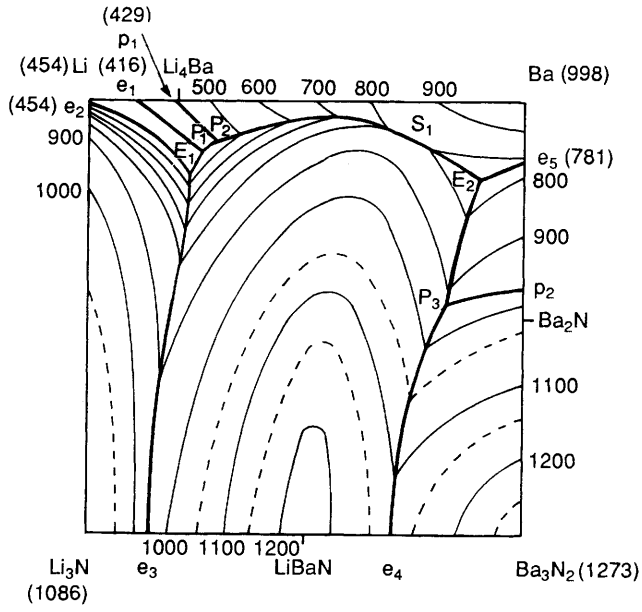


**Fig. 1** Space model (isothermal contour diagram) for the Li–Ba–$Ba_3N_2$–$Li_3N$ pseudo-quaternary phase diagram based on known data for the four constituent binary systems and consistent with the results reported here. Quoted temperatures (K) are those of invariant points in the binary systems. The isotherms are at 100 K intervals, except for those shown as dashed lines which are at 50 K intervals

## Experimental

The apparatus and procedure for the measurement of the resistance of homogeneous liquid metal solutions have been described previously.[37] A version of the capillary method was employed in which a thread of liquid metal was circulated continuously from the vessel reservoir through a narrow bore (i.d. 3.0 mm) loop using a miniature electromagnetic pump. Circulation of the metal also served to ensure thorough mixing of the metal mixture and to present a clean metal surface for reaction with gaseous nitrogen. The resistance of the solution was determined when passing through the loop, using a version of the four-point probe method.[37] It was monitored as a function of nitrogen concentration under isothermal conditions. Resistivities ($\pm 0.1 \times 10^{-8}$ Ω m) were calculated from calibration and sample resistance data and the dimensions of the capillary.[37] The vessel, of all-welded stainless steel (AISI 316) construction, except for the glass facility for attachment to the vacuum frame, was located in an air oven, fitted with an internal circulation fan and a proportional band controller (± 0.5 K at 673 K). The temperature of the capillary was measured using four pre-calibrated chromel-alumel thermocouples, attached to the capillary. The neck of the vessel and the electrical and thermocouple leads projected through the oven roof for attachment to the vacuum frame and electrical equipment, as appropriate.

A similar, less complex, vessel was used for the kinetic and thermal analysis studies. Instead of the resistivity capillary, a small loop constructed from wider bore (i.d. 7.0 mm) tubing was attached to the miniature magnetic pump for circulation of the metal. Located in the base of the vessel was a pocket into which a chromel–alumel thermocouple (± 1 K) was inserted after calibration.

The metal mixtures were prepared *in situ* by weighing in the appropriate alkaline-earth metal [calcium (Koch Light; purity 99.9%; 2–10 g), strontium (Koch Light; purity 99.9%; 4–40 g) and barium (Koch Light; purity 99.9%; 7–30 g)] to the liquid lithium (Koch Light; purity, 99.98%; ≈30 g). Argon (Air Products; purity 99.99%) was used to protect the liquid metal at all times. The alkaline-earth metals were prepared in the form of small rectangular blocks (≈5 × ≈5 × ≈20 mm) from as received samples by sawing under liquid paraffin oil. Initial

purification of the alkaline-earth metals involved removal of surface contaminants (paraffin oil, oxides, nitrides, *etc.*) by immersion in dilute acetic acid. Final purification, carried out in an evacuable glove box, involved mechanical removal of the remaining surface contamination by filing until a bright, shiny, metallic surface was achieved. Subsequently, the alkaline-earth metals were handled in purified argon. Lithium and argon were purified as described previously.[37]

Nitrogen (Air Products, 99.98%), purified by passage through molecular sieve and manganese(II) oxide, was exposed in small volumes ($\approx 10^4$ mm$^3$ at standard temperature and pressure) to the metal under isothermal conditions. Its reaction with the metal mixture was monitored by pressure measurement and, in the case of the resistivity experiments, by resistance measurement. When equilibrium had been attained, either the gas addition was repeated (for the resistivity and kinetic studies) or the vessel was filled with argon and a cooling curve obtained (for the thermal studies). After completion of the experiments some vessels were sawn open in an argon filled glove-box and samples taken for X-ray powder diffraction analysis; the products were studied in the metal matrix as distillation of excess metal would have disturbed the equilibrium. It is pertinent that in those vessels used for prolonged experiments, the metal had a tendency to creep up the walls of the reservoir.

## Results and Discussion

(*i*) *Electrical Resistivity Experiments.*—Equilibrium resistivity–composition data were obtained for the addition of 38 aliquots of nitrogen to a hypoeutectic Li–Ba alloy (initial $x_{Ba}$ = 0.0259) under isothermal conditions (673 K). The results are shown in Fig. 2 (ABCD), where they are compared to the corresponding data obtained for the addition of nitrogen to pure lithium (AXY).[33] As the nitrogen is added, the resistivity exhibits an initial increase, attributed to a solution process, followed by an effectively constant section, attributed to a precipitation process. For the ternary system, the increase can be split into two sections. For dilute solutions, the increase is small and non-linear with an increasing gradient (section AB); it is only for more concentrated nitrogen solutions that a linear increase in resistivity is observed. The gradient of this latter section (section BC) is considerably smaller [$5.6 \times 10^{-8}$ Ω m (atom%)$^{-1}$] than that (section AX) for the binary system [$7.0 \times 10^{-8}$ Ω m (atom%)$^{-1}$] which is linear throughout, inferring that the solution process involves not only dissolution of the nitrogen but also interaction with dissolved barium. The marked change at point C, when the resistivity becomes effectively constant (section CD), represents a saturation point in the system. The nitrogen concentration at saturation in the Li–Ba–N system (point C; $x_{Ba}$ = 0.0251; $x_N$ = 0.0306; [N]/[Ba] = 1.22) is much higher than in the Li–N system (point X; $x_N$ = 0.0145), again suggesting that dissolved barium plays a significant role in the solution process.

The product which precipitates from the binary system has previously been shown to be $Li_3N$;[33–35] that which precipitates from the ternary system could be one of three phases, $Li_3N$, LiBaN or $Ba_2N$. By comparison of the experimental resistivity data obtained after saturation with those predicted for saturation of these three phases, the identity of the precipitate can ascertained. The analysis is included in Fig. 2. If $Li_3N$ is precipitated the resistivity should increase (line CE) as the barium concentration of the solution increases owing to loss of lithium. Resistivity decreases would occur if the precipitate were to contain barium; that expected for LiBaN is shown by line CF, that for $Ba_2N$ by line CG. Comparison of the experimental results with the three possibilities suggests that $Li_3N$ is the precipitating phase.

These observations indicate that the $Li_3N$ precipitation face extends into the pseudo-quaternary phase diagram from the Li–$Li_3N$ edge, the solubility of $Li_3N$ increasing with increasing barium content (Fig. 1).

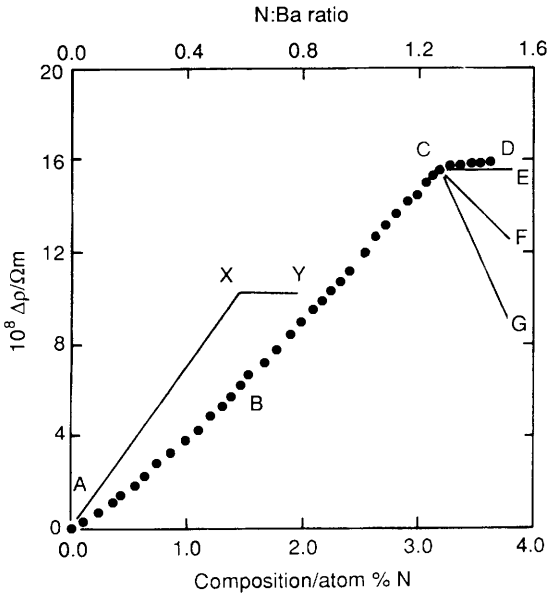


**Fig. 2** Comparison of the resistivity changes observed at 673 K on addition of nitrogen to a hypoeutectic Li–Ba alloy (initial $x_{Ba}$ = 0.029) (ABCD) and to pure lithium (AXY) showing the predicted resistivity changes on precipitation of $Li_3N$ (CE), LiBaN (CF) and $Ba_2N$ (CG)

(*ii*) *X-Ray Diffraction Experiments.*—Despite many attempts, high quality X-ray powder diffraction patterns of the products could not be obtained owing to the fact that they were embedded in a solid metal matrix. Nonetheless, they were of sufficient quality to confirm the presence of not only $Li_3N$[38] but also LiBaN;[31] there was no evidence for $Ba_2N$ or $Ba_3N_2$ formation. The presence of both $Li_3N$ and LiBaN in the metal matrix suggests that the ternary invariant eutectic involves solidification of lithium, $Li_3N$ and LiBaN (Fig. 1).

(*iii*) *Kinetic Experiments.*—Nitrogen absorption by a hypoeutectic Li–Ba alloy (initial $x_{Ba}$ = 0.080) was monitored for a total of 20 aliquots under isothermal conditions ($T$ = 438 K); the amount of nitrogen added in each aliquot was chosen to increase the nitrogen content of the system by ≈0.1 atom% N. As the reaction is quite rapid, nitrogen pressure ($p_{N_2}$) was measured at 5 s intervals. Typical $p_{N_2}$–time curves are shown in Fig. 3. As shown by the linearity of the corresponding ln $p_{N_2}$–time plots (Fig. 3), they are first order with respect to nitrogen. The curves fall into two sections as shown by the variation of their first-order rate constants ($k_p$), equation (5), as a function

$$dp_{N_2}/dt = -k_p t \qquad (5)$$

of [N]/[Ba] ratio (Fig. 4). The rate constants of the first 14 curves are very similar lying in the range $7.6 \times 10^{-2}$ to $9.7 \times 10^{-2}$ s$^{-1}$. Those for the later curves decrease markedly with increasing nitrogen content. A similar pattern was observed in a detailed study of the kinetics of the reaction of nitrogen with sodium–barium solutions,[39] where the change in behaviour was attributed to the generation of solid product. Hence the break in the $k_p$–[N]/[Ba] ratio plot, which occurs at [N]/[Ba] = 0.36, is assumed to correlate to the solubility limit of $Li_3N$ in this system ($x_N$ = 0.0288).

In a separate series of experiments starting with a hypoeutectic Li–Ba alloy containing 2.59 atom% Ba, the variation of the rate constant as a function of temperature ($413 \leqslant T/K \leqslant 526$) was determined. To ensure the validity of the results, the rate-constant measurements were duplicated on increasing and decreasing temperature. The Arrhenius plot summarising these results is shown in Fig. 5. The data are best represented by equation (6) which gives an activation energy of 33.6 kJ mol$^{-1}$.

**Table 1** Solubility data (atom%) for nitrogen in dilute solutions of barium in liquid lithium

| $T$ = 673 K | | | | ≈430 K | | | | |
|---|---|---|---|---|---|---|---|---|
| [Ba]$^a$ | [Ba]$^b$ | [N]$^b$ | [N]/[Ba]$^b$ | $T$ | [Ba]$^a$ | [Ba]$^b$ | [N]$^b$ | [N]/[Ba]$^b$ |
| 0.00 | 0.00 | 1.53 | — | 454 | 0.00 | 0.00 | 0.03 | — |
| 2.59 | 2.51 | 3.06 | 1.22 | 438 | 4.75 | 4.69 | 1.19 | 0.26 |
| | | | | 430 | 7.51 | 7.34 | 2.25 | 0.31 |
| | | | | 438 | 8.00 | 7.77 | 2.88 | 0.38 |
| | | | | 405 | 13.20 | 12.06 | 8.58 | 0.78 |

$^a$ Initial. $^b$ At saturation.

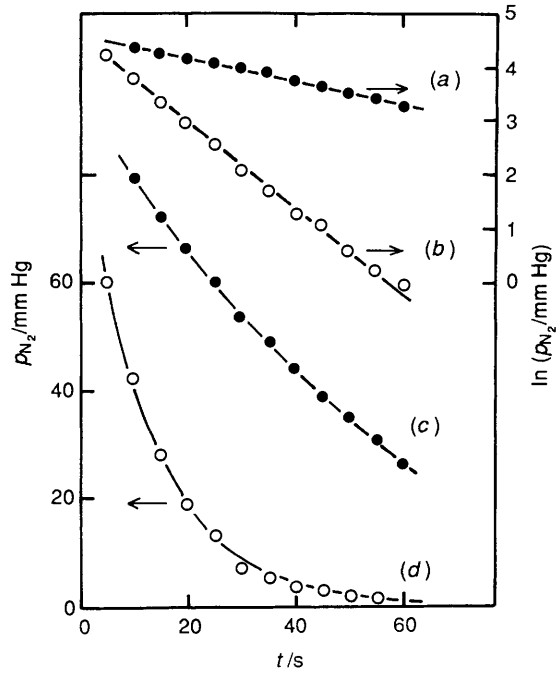


**Fig. 3** Pressure- and ln(pressure)–time relationships at 438 K for two aliquots of nitrogen added to a hypoeutectic Li–Ba alloy (initial $x_{Ba}$ = 0.08). N:Ba = 0.48 (*a*), (*c*) or 0.30 (*b*), (*d*); mmHg ≈ 133 Pa

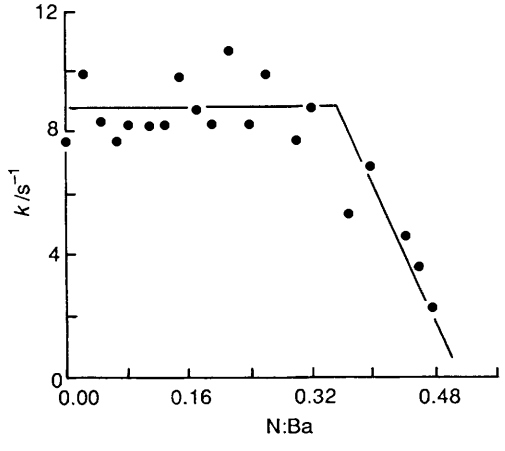


**Fig. 4** Variation of the first-order rate constants for a series of nitrogen aliquots added to a hypoeutectic Li–Ba alloy (initial $x_{Ba}$ = 0.08) as a function of N:Ba ratio

$$\ln(k_p/\text{mmHg}) = -4040(T/\text{K})^{-1} + 5.618 \quad R^2 = 0.961 \quad (6)$$

Although the solubility obtained by this method ($x_N$ = 0.0288) is consistent with those obtained using the other techniques (Table 1), the method was not pursued. Its accuracy

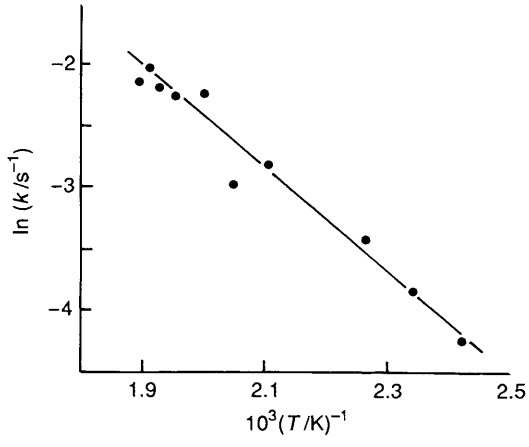


**Fig. 5** Arrhenius plot for the first-order rate constants of the reaction of nitrogen with a hypoeutectic Li–Ba alloy (initial $x_{Ba}$ = 0.0259)

was limited not only by the variation of the rate constant over the initial section (Fig. 4) but also by changes which occurred when the experiment was either left for a period or subjected to thermal analysis. After ageing or thermal analysis, abnormally fast reaction rates were observed; they were attributed to large increases in surface area noted when vessels were cut open at the end of the experiment. The two series of experiments described in this section were carried out in very limited time scales to minimise effects due to surface area changes.

(*iv*) *Thermal Analysis Experiments.*—Phase relationships at the lithium corner of the Li–Ba–N ternary system were investigated by examining four vertical sections. The compositions of the Li–Ba solutions (initial $x_{Ba}$ = 0.0475, 0.0751, 0.132 and 0.1391) were chosen to straddle the eutectic of the Li–Ba system ($x_{Ba}$ = 0.105; $T$ = 416 K);[26,27] the amount of nitrogen added in each aliquot was chosen to increase the nitrogen content of the system by ≈0.05 atom% N. After each nitrogen aliquot the solution was subjected to thermal analysis to determine the sequence of phase changes. The data points obtained on addition of nitrogen to the four solutions are shown in Figs. 6–9. Although complete sets of data were obtained for the first three solutions (Figs. 6–8; $[N]/[Ba]_{max}$ = 0.8), only limited results were obtained for the fourth solution (Fig. 9; $[N]/[Ba]_{max}$ = 0.12) owing to premature failure of the reaction vessel.

The results from the thermal analysis studies can be considered as vertical sections through the Ba–$Ba_3N_2$–$Li_3N$–Li space model (Fig. 1). The phase regions included on the four vertical sections (Figs. 6–9) are derived from the space model. The location of the two phase (Li + LiBaN) region cannot be defined rigorously, owing to the slow kinetics of the quasi-peritectic conversion of $Li_4Ba$ into LiBaN; however, for completeness, its approximate location is shown in all four figures.

For dilute solutions of nitrogen in the hypoeutectic Li–Ba solutions (initial $x_{Ba}$ = 0.0475 and 0.0751; Figs. 6 and 7,

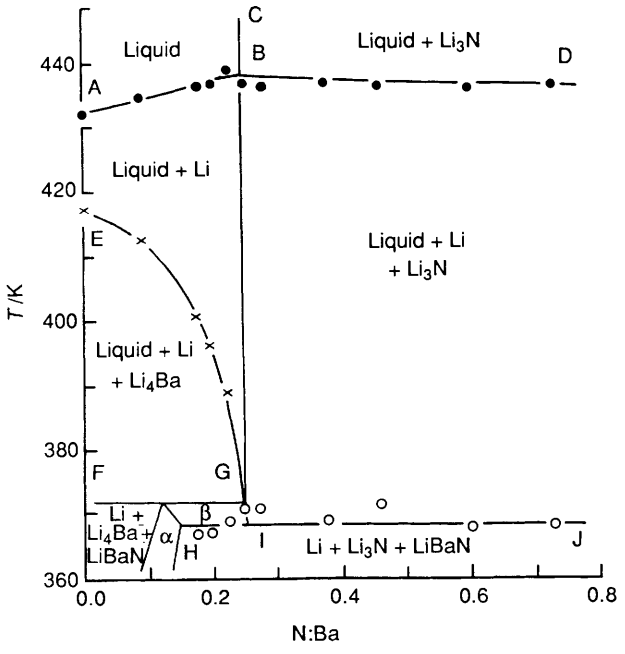


**Fig. 6** Vertical section through the pseudo-quaternary phase diagram, derived from thermal analytical data for the addition of nitrogen to a hypoeutectic Li–Ba alloy (initial $x_{Ba}$ = 0.0475) (Phase fields: α = Li + LiBaN; β = liquid + Li + LiBaN)

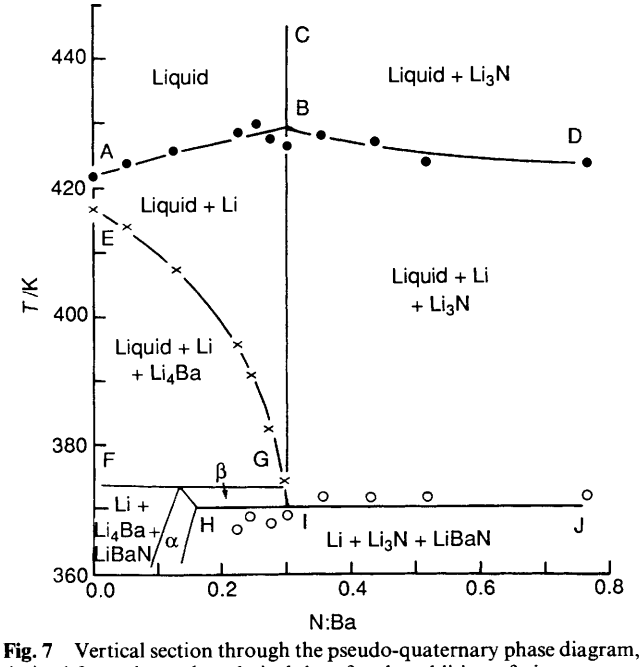


**Fig. 7** Vertical section through the pseudo-quaternary phase diagram, derived from thermal analytical data for the addition of nitrogen to a hypoeutectic Li–Ba alloy (initial $x_{Ba}$ = 0.0751) (Phase fields: α = Li + LiBaN; β = liquid + Li + LiBaN)

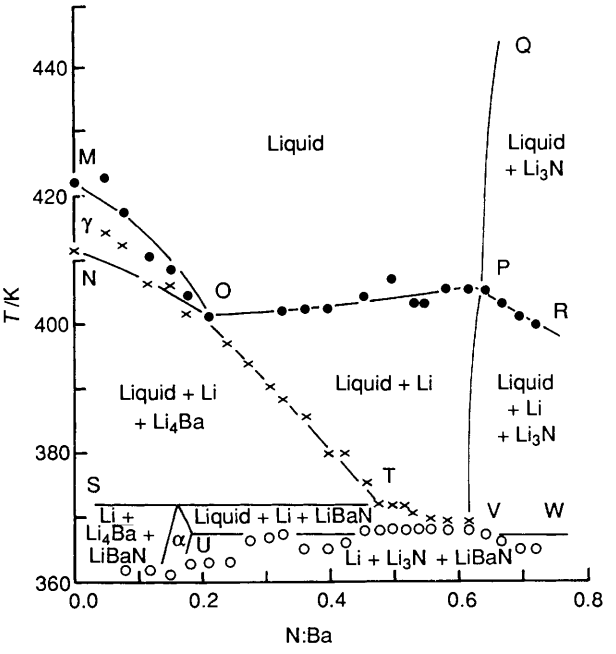


**Fig. 8** Vertical section through the pseudo-quaternary phase diagram, derived from thermal analytical data for the addition of nitrogen to a hypereutectic Li–Ba alloy (initial $x_{Ba}$ = 0.1320) (Phase fields: α = Li + LiBaN; γ = liquid + $Li_4Ba$)

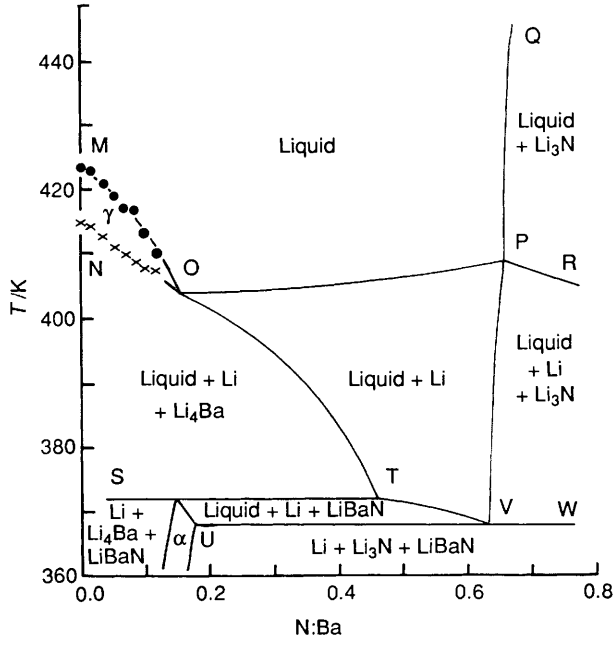


**Fig. 9** Vertical section through the pseudo-quaternary phase diagram, derived from thermal analytical data for the addition of nitrogen to a hypereutectic Li–Ba alloy (initial $x_{Ba}$ = 0.1391) (Phase fields: α = Li + LiBaN; γ = liquid + $Li_4Ba$)

respectively), the first phase boundary (line AB) represents the crystallisation of pure lithium; the second (line EG) the solidification of the binary Li–$Li_4Ba$ eutectic mixture and the third (line HI) the freezing of the ternary Li–$Li_4Ba$–LiBaN eutectic mixture. The temperatures at which the first two thermal effects occur diverge with increasing nitrogen content. The third thermal arrest is independent of composition, invariably occurring at ≈368 K. The quasi-peritectic conversion of $Li_4Ba$ into LiBaN (line FG) is not observed, probably owing to its slow kinetics. If equilibrium is not achieved, the solidification of the ternary eutectic will be observed instead. The presence of the quasi-peritectic reaction is required to rationalise the other thermal analytical data as well as the presence of LiBaN in the solid products. For more concentrated nitrogen solutions only two thermal effects are observed. The first (line BD), which slowly decreases in temperature with increasing nitrogen content, is attributed to the solidification of the binary Li–$Li_3N$ eutectic mixture; the second (line IJ), which is essentially independent of concentration, corresponds to the ternary eutectic reaction. The $Li_3N$ crystallisation face (line BC) is not observed for these solutions. Since the hypereutectic liquidus of the Li–$Li_3N$ binary system is very steep, it is assumed that the $Li_3N$ crystallisation face will be similarly steep. The

very small heat evolution associated with such a steep phase boundary will not be detectable. Its presence is confirmed, however, by the resistivity and kinetics results.

For dilute solutions of nitrogen in the hypereutectic Li–Ba solutions (initial $x_{Ba} = 0.132$ and 0.1391; Figs. 8 and 9, respectively), the first phase boundary (line MO) represents the crystallisation of $Li_4Ba$, the second (line NO) the solidification of the binary Li–$Li_4Ba$ eutectic mixture and the third (line UV) to the freezing of the ternary Li–$Li_4Ba$–LiBaN eutectic mixture. The temperatures at which the first two thermal effects occur converge with increasing nitrogen content, meeting at point O ($x_{Ba} = 0.1284$, $x_N = 0.0269$; [N]/[Ba] = 0.21; 401 K). The third thermal arrest is independent of composition, invariably occurring at ≈368 K. As for the hypoeutectic solutions, the quasi-peritectic reaction involving conversion of $Li_4Ba$ into LiBaN (line ST) is not observed. For more concentrated nitrogen solutions, three thermal effects are again observed, but in this case the first two diverge. The first (line OP) increases slightly to a maximum at point P, while the second (line OTV) falls quite rapidly to the temperature of the pseudo-peritectic reaction at point T and then more slowly to the ternary eutectic reaction at point V. The third thermal arrest (line UV) is independent of temperature, occurring at ≈368 K. The first (line OP) is attributed to the crystallisation of lithium; the second (line OTV) to the precipitation of first (section OT) the binary Li–$Li_4Ba$ eutectic and secondly (section TV) the binary Li–LiBaN eutectic, and the third to the solidification of the ternary Li–$Li_3N$–LiBaN eutectic mixture. At even higher nitrogen contents, only two arrests are observed. The first (line PR) corresponds to the precipitation of $Li_3N$–LiBaN mixtures, while the second (line VW) is attributed to the solidification of the ternary Li–$Li_3N$–LiBaN eutectic mixture. As before, the $Li_3N$ crystallisation face (line PQ) is not observed for these solutions.

These results indicate that the initial product of the reaction is $Li_3N$ for all solutions containing up to $x_{Ba} = \approx 0.14$; hence, the monovariant line ($e_3E_1$) joining the $Li_3N$–LiBaN binary eutectic ($e_3$) to the ternary eutectic ($E_1$) must lie at higher barium content (Fig. 1). LiBaN is only formed on cooling through the ternary eutectic reaction. The location of the $Li_3N$ crystallisation face on the space model (Fig. 1) is given by the variation in the nitrogen solubility as a function of barium content. The present data, obtained at ≈430 K and 673 K, are collated together with the solubility of nitrogen in liquid lithium in Table 1. Nitrogen solubility increases with both temperature and barium content; however, the [N]/[Ba] ratio passes through a minimum with increasing barium content giving a convex shape to the $Li_3N$ crystallisation face. This is shown in Fig. 10, a more detailed representation of the lithium-rich corner of the pseudo-quaternary system. The points shown, taken directly from the vertical sections (Figs. 7–9), represent the composition dependence of the monovariant lines formed by the intersection of the lithium and $Li_4Ba$, and of the lithium and $Li_3N$, crystallisation fields. Extrapolation of these lines and inclusion of the other three monovariant lines associated with the lithium, $Li_4Ba$, $Li_3N$ and LiBaN crystallisation fields gives an indication of the relative locations of the pseudo-peritectic and ternary eutectic points ($P_1$ and $E_1$).

## Conclusion

The reaction of nitrogen with liquid lithium containing dissolved barium follows a solution–precipitation mechanism. Initially, nitrogen dissolves in the liquid metal to form an homogeneous solution; the reaction is first order with respect to nitrogen with an activation energy of 33.6 kJ $mol^{-1}$. Subsequently, it reacts to form a precipitate of $Li_3N$; the $Li_3N$ crystallisation face is dependent on the barium content of the solution, nitrogen solubility rising with increasing barium content. The ternary nitride, LiBaN, is only formed on cooling the solution; there is no evidence for $Ba_2N$ or $Ba_3N_2$ formation.

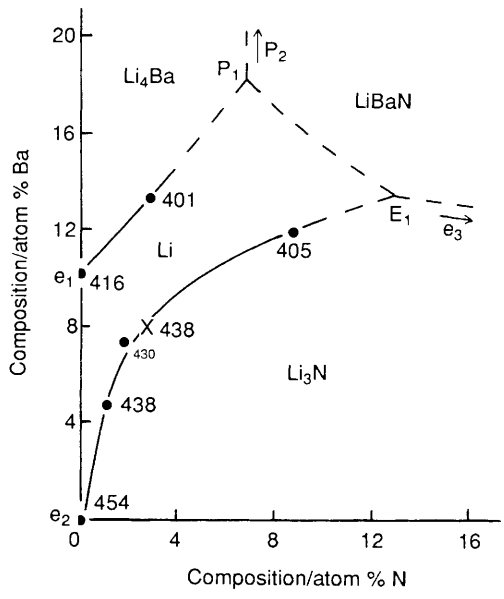


**Fig. 10** Detailed representation of the lithium-rich corner of the pseudo-quaternary phase diagram, showing the invariant points derived from the vertical sections (●) and the nitrogen solubility derived from the kinetic studies ( × ) (temperatures/K given against the point). The formulae shown identify the four crystallisation faces

This behaviour pattern is different from that in the corresponding Na–M–N (M = Sr or Ba) systems where the solubility is directly proportional to the alkaline-earth metal content of the solution and the precipitating phase is the alkaline-earth metal subnitride, $M_2N$ (M = Sr or Ba). The difference in behaviour can be directly related to the relative thermodynamic stabilities of $Li_3N$ and $Na_3N$.

Preliminary results[40] from other systems, namely the Li–Ca–N and Li–Sr–N systems, indicate that of the three alkaline-earth metals, barium is the most effective in solubilising nitrogen and calcium least effective. For example, at 673 K and a concentration ($x_M$) of 0.050 for the alkaline-earth metals, the concentration of nitrogen ($x_N$) is 0.047 in the Li–Ba–N system (extrapolated results), 0.035 in the Li–Sr–N system[40] and 0.025 in the Li–Ca–N system.[40]

## Acknowledgements

We would like to thank the SERC for financial support (to P. G. R.).

## References

1 R. J. Pulham and P. Hubberstey, *J. Nucl. Mater.*, 1983, **115**, 239.
2 M. W. Chase, C. A. Davies, J. R. Downey, D. J. Frurip, R. A. McDonald and A. N. Syverud, *J. Phys. Chem. Ref. Data*, 1985, **14**, Suppl. 1.
3 C. C. Addison, *The Chemistry of the Alkali Metals*, Wiley, Chichester, 1984.
4 M. G. Barker, P. G. Gadd and M. J. Begley, *J. Chem. Soc., Dalton Trans.*, 1984, 1139.
5 M. G. Barker and D. J. Wood, *J. Less Common Metals*, 1974, **35**, 315.
6 A. T. Dadd and P. Hubberstey, *J. Chem. Soc., Dalton Trans.*, 1982, 2175.
7 P. Hubberstey and A. T. Dadd, *J. Nucl. Mater.*, 1983, **122** and **123**, 1231.
8 P. Hubberstey, in *Proc. Third Int. Conf. Liquid Metal Engineering and Technology*, British Nuclear Energy Society, Oxford, 1984, vol. 2, p. 85.
9 P. Hubberstey and P. G. Roberts, *J. Nucl. Mater.*, 1988, **155–157**, 694.
10 M. G. Barker, P. Hubberstey, A. T. Dadd and D. A. Frankham, *J. Nucl. Mater.*, 1983, **114**, 143.
11 P. Hubberstey and P. G. Roberts, *J. Nucl. Mater.*, 1984, **120**, 74.
12 G. J. Moody and J. D. R. Thomas, *J. Chem. Educ.*, 1966, **43**, 205.

13 R. N. Anderson and N. A. D. Parlee, *High Temp. Sci.*, 1970, **2**, 289.
14 P. Hubberstey, *Proc. Int. Conf. Liquid Alkali Metals*, British Nuclear Energy Society, London, 1973, vol. 1, pp. 15–19.
15 C. C. Addison, R. J. Pulham and E. A. Trevillion, *J. Chem. Soc., Dalton Trans.*, 1975, 2082.
16 C. C. Addison, G. K. Creffield, P. Hubberstey and R. J. Pulham, *J. Chem. Soc., Dalton Trans.*, 1976, 1105.
17 P. Hubberstey and P. R. Bussey, *Proc. Int. Conf. Liquid Metal Engineering and Technology*, British Nuclear Energy Society, London, 1984, vol. 3, p. 143.
18 P. Gross, G. L. Wilson and W. A. Gutteridge, *J. Chem. Soc. A*, 1970, 1908.
19 P. Hubberstey and T. Sample, *J. Nucl. Mater.*, 1992, **191–194**, 277.
20 G. Casini, P. Labbe, M. Reiger, L. Barraer, M. Biggio, F. Farfaletti-Casali, G. Gervaise, L. Giancarli, M. Roze, Y. Severi, J. Quintric-Bossy, S. Tominetti, J. Wu and M. Zucchetti, *Fusion Eng. Des.*, 1991, **14**, 353.
21 S. Malang, H. Deckers, U. Fischer, H. John, R. Meyder, P. Norajitra, J. Reimann, H. Reiser and K. Rust, *Fusion Eng. Des.*, 1991, **14**, 373.
22 M. G. Barker, J. A. Lees, T. Sample and P. Hubberstey, *J. Nucl. Mater.*, 1991, **179–181**, 599.
23 C. C. Addison, *Sci. Prog. Oxf.*, 1972, **60**, 385.
24 E. Veleckis, K. E. Anderson, F. A. Cafasso and H. M. Feder, USAEC Report, ANL-7520 (part I), 1968, p. 295.
25 P. E. Rauch and A. Simon, *Angew. Chem., Int. Ed. Engl.*, 1992, **31**, 1519.
26 D. V. Keller, F. A. Kanda and A. J. King, *J. Phys. Chem.*, 1958, **62**, 732.
27 A. D. Pelton, *Bull. Alloy Phase Diagrams*, 1984, **5**, 452.
28 V. A. Russell, M.Sc. Thesis, University of Syracuse, New York, 1949.
29 R. H. Orcutt, *J. Res. Nat. Bur. Stand., Sect. A*, 1970, **74**, 45.
30 S. M. Ariya, *J. Gen. Chem. USSR*, 1955, **25**, 609.
31 J. F. Bryce and J. Aubry, *C. R. Hebd. Seances Acad. Sci.*, 1970, **271**, 825.
32 M. G. Barker, personal communication.
33 P. F. Adams, M. D. Down, P. Hubberstey and R. J. Pulham, *J. Less-Common Met.*, 1975, **42**, 325.
34 K. A. Bolshakov, P. I. Fedorov and L. Stepina, *Izv. Vyssh. Uchebn. Zaved., Tsvetn. Metall.*, 1959, 52.
35 R. M. Yonco, E. Veleckis and V. A. Maroni, *J. Nucl. Mater.*, 1975, **57**, 317.
36 P. Hubberstey, R. J. Pulham and A. E. Thunder, *J. Chem. Soc., Faraday Trans. 1*, 1976, 431.
37 P. Hubberstey, M. G. Barker and T. Sample, *Fusion Eng. Des.*, 1991, **14**, 227.
38 A. Rabenau and H. Schulz, *J. Less-Common Met.*, 1976. **50**, 155.
39 G. T. Lindley, Ph.D. Thesis, University of Nottingham, 1969.
40 P. Hubberstey and P. G. Roberts, in *Liquid Metal Systems II*, ed. H. U. Borgstedt, Plenum Press, New York, in the press.

*Received* 26*th August* 1993; *Paper* 3/05157F